Enhanced colloidal monolayer assembly via vibration-assisted convective deposition

Tanyakorn Muangnapoh, Alexander L. Weldon, and James F. Gilchrist

Citation: Applied Physics Letters **103**, 181603 (2013); doi: 10.1063/1.4825351
View online: http://dx.doi.org/10.1063/1.4825351
View Table of Contents: http://scitation.aip.org/content/aip/journal/apl/103/18?ver=pdfcov
Published by the AIP Publishing

Enhanced colloidal monolayer assembly via vibration-assisted convective deposition

Tanyakorn Muangnapoh, Alexander L. Weldon, and James F. Gilchrist[a)]
Department of Chemical Engineering, Lehigh University, Bethlehem, Pennsylvania 18015, USA

(Received 4 August 2013; accepted 2 October 2013; published online 29 October 2013)

We demonstrate a purely mechanical technique for enhancing evaporation-driven convective deposition of particle monolayers from suspension. Lateral vibration in the deposition direction results in monolayer deposition at faster speeds, over a wider range of withdraw rates, and with higher order versus traditional convective deposition. These enhancements and phenomena are a result of variation in the thin film, where capillary interactions result in self-assembly by dynamically changing the air-liquid interface. This enhancement in fabricating ordered particle thin films may enable development of optical and biological applications and efforts to scale-up this process for commercial application. © *2013 AIP Publishing LLC*. [http://dx.doi.org/10.1063/1.4825351]

Convective deposition, the evaporation-driven flow and capillary-driven assembly of colloidal particles on a substrate, for creating an ordered particle monolayer has proven successful across varying applications ranging from the fabrication of microlens arrays for light emitting diodess,[1–6] membranes,[7] surfaces with controlled roughness,[8] and fabrication of janus particles.[9] Convective deposition essentially combines two recently explained concepts. The first, commonly known as the "coffee ring" effect,[10] describes the phenomenon where particles flow to the contact line of a meniscus as a result of the evaporative flux.[11–13] Convective deposition shares similar physics to these evaporating droplets as a suspension droplet is dragged across a substrate. This results in a trailing drawn-out thin film with enhanced evaporation. Particles are drawn into this region from the bulk and then are confined in a 2D thin film where they locally deform the liquid-air interface. Minimizing surface energy, the particles experience strong capillary-driven forces that result in particle-particle and particle-substrate attractive potential. The inter-particle interactions, previously described by Gifford and Scriven,[14] were coined the "cheerio effect."[15] This describes the macroscopic phenomena of particle attractions as a result of interface deflections coming from their contact lines, relative buoyancy, and/or vertical confinement. The inter-particle interactions are strong and pull particles into their maximum packing density within the thin film. Capillary forces are sufficiently strong to overcome particle-particle and substrate-particle electrostatic repulsion and bring particles into contact with each other and the substrate. These same experimental conditions can be used to deposit particle multilayers in the form of a colloidal crystal where the physics of assembly depends on confinement and flow steering[16] as opposed to surface energy.

Previous work on convective deposition includes early work by Nagayama[12] and coworkers who, through a simple mass balance, calculated the withdraw velocity u_d that matches the crystallization velocity u_c,

$$u_d = u_c = \frac{J_e \phi}{0.605 d(1-\phi)}, \tag{1}$$

that depends on the particle volume fraction ϕ, evaporation flux J_e of the liquid medium, and particle diameter d. Previous enhancements to the convective deposition process have aimed at altering suspension and surface properties. Process enhancements aiming to increase its robustness, repeatability, and scale-up potential have been lacking.

Here, a substantial enhancement of the convective deposition process is presented in the addition of periodic vibration in the direction of substrate motion. The schematic diagram, shown in Fig. 1(a), is similar to that for traditional convective deposition except for the added ability to oscillate the substrate along the deposition direction (Fig. 1(b)). The original motivation for this work was to investigate how noise would affect convective deposition and whether vibration would thwart efforts to scale up this process in a commercial setting. Investigation into the stability of a vibrating, falling film is a classic problem.[17–19] Additionally, more recent studies have used vibration to influence colloidal assembly.[20,21] Notably, work by Wei and coworkers[22] demonstrates that vibration of a monolayer of particles confined in a vertical soap film can anneal defects with a logarithmic coarsening profile; however, the time scales in this work are inappropriately long for convective deposition due to the short particle residence time in the thin film and their scale-up limitations.

We present intriguing results showing enhanced convective deposition through increased viable deposition speeds, enhanced robustness of the deposition process through transition to a monolayer-deposition window, and higher resultant packing and order of deposited monolayers. These enhancements occur over a large range of vibration frequencies and amplitudes. While flow kinematics have likely evolved beyond simple explanation, we hypothesize a phenomenological understanding of these changing properties.

The primary aqueous colloid suspension of 20% by volume of 1 μm silica and 8% by volume 75 nm polystyrene nanoparticles used in this work is prepared as described in previous work.[23,24] A plain glass microslide

[a)]Author to whom correspondence should be addressed. Electronic mail: gilchrist@lehigh.edu

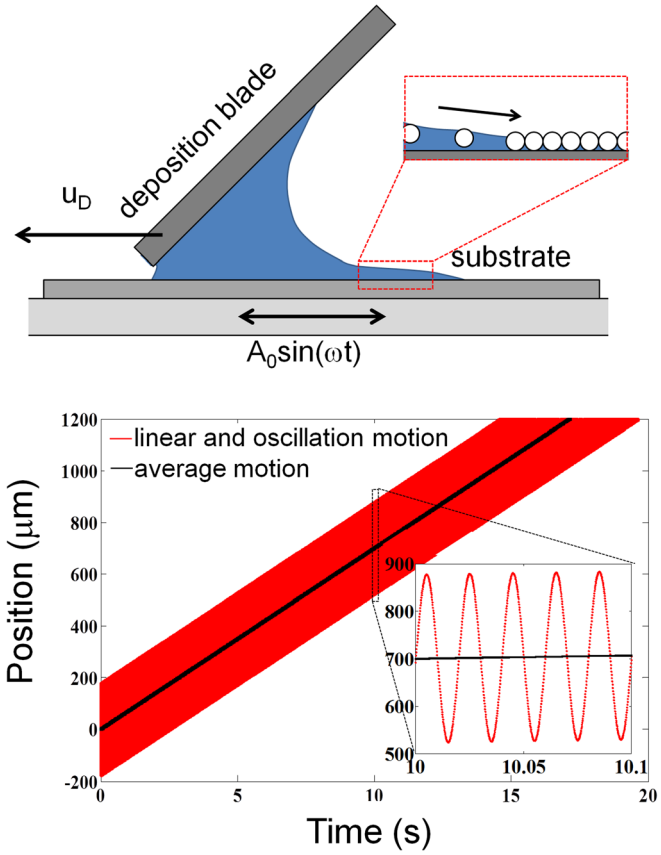

FIG. 1. Schematic diagram of experimental setup showing deposition apparatus with a substrate motion highlighted and a graph of substrate motion.

(76 × 25 × 1 mm, Fisher PA) is used as the deposition blade and glass cover slides (40 × 24 × 0.25 mm, Fisher PA) are used as substrates in all experiments. Deposition blades are hydrophobically treated with the addition of parafilm to their bottom edge as described previously.[1] All glass substrates are immersed in Piranha solution, 5:1 V/V sulfuric acid/hydrogen peroxide, used as a cleaning agent, for at least 3 h then rinsed and stored in DI water. The experimental setup is shown in Fig. 1. This apparatus is contained within a humidity-controlled environment, where all experiments are performed at 20% relative humidity and 24 °C. The blade angle is set at 45° approximately 10 μm above the substrate. The motion of the substrate is controlled through a linear motor (Harvard Instruments Co. Ltd.), while a mechanical driver (PASCO SF-9324) and a waveform generator (Agilent 3320A) are used to control periodic oscillation. The position of the substrate is given by $x = u_D t + A_0 \sin\omega t$, where u_D is the apparent deposition velocity of the substrate and A_0 and ω are the amplitude and frequency of vibration. The relative velocity and acceleration of the sinusoidal motion scale as $A_0\omega$ and $A_0\omega^2$, respectively.

Deposited monolayers are observed directly using SEM (Hitachi 4300) after iridium coating and through confocal laser scanning microscopy after rewetting the layer with an aqueous solution of 8 mM Rhodamine B. Optical imaging of the sample was automated along the deposition length sampling ~60 000 microspheres. The relative microsphere substrate coverage, ρ, and the local bond order, Ψ_6, were evaluated. The maximum theoretical value of surface coverage for monosized microspheres deposited as a two-dimensional hexagonally close packed (HCP) crystal is $\rho = \frac{\pi}{(\sqrt{12})^2} = 0.907$. The long-range microsphere substrate coverage is qualitatively reported. Ψ_6 is a parameter describing the relative crystallinity of particles. It is calculated using angles θ between each particle of interest i and their nearest neighbors j. Vectors r_{ij} are determined for all nearest neighbors N and Ψ_6 is defined as

$$\Psi_6(r_{ij}) = \frac{1}{N}\sum_{j=1}^{N} \exp[6i\theta(r_{ij})], \tag{2}$$

where $\Psi_6 = 1$ describes particles oriented in a perfect hexagonally close-packed crystal. A monolayer is seen as having $\rho \geq 0.8$ and $\Psi_6 \geq 0.575$. Submonolayers have densities $\rho < 0.8$ and multilayer depositions are identified through direct imaging of multiple layers or through increased light reflectance.

Glass substrates were coated using variable deposition velocity, $0 \leq u < 90$ μm/s, vibration amplitude, $0 \leq A_0 < 300$ μm, and frequency $1 \leq \omega \leq 50$ Hz. Similar to traditional convective deposition (effectively where $A_0 = 0$ (Ref. 24)), at optimum conditions relatively large areas are easily coated with a small amount of solution in a uniform fashion, shown on a coated glass slide (Fig. 2(a)). Qualitatively, at the macroscopic scale three observations are apparent even with the smallest vibration amplitudes sampled ($A_0 > 10$ μm). First, the quality of coated substrates appears more uniform and over a larger area than those coated using traditional, constant velocity, convective deposition. Second, buildup of particles near the edges of the coated area and the formation of streaks of multilayers propagating in the direction of deposition are minimized with the vibration frequencies sampled. Third, although not investigated thoroughly for this study, substrates of variable hydrophobicity

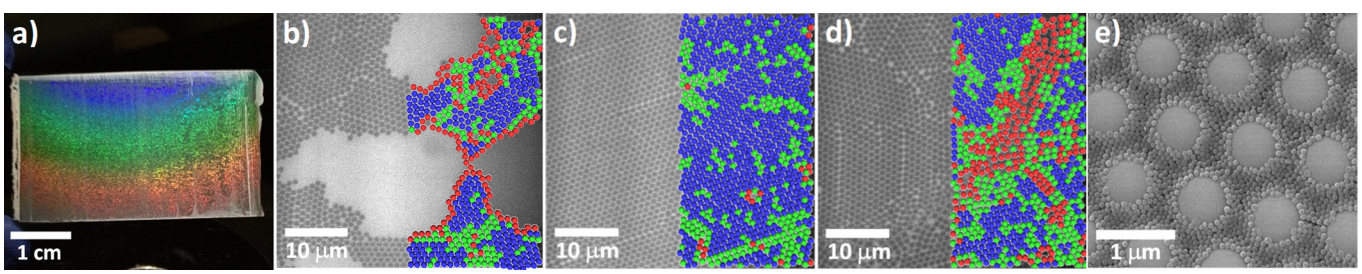

FIG. 2. Examples of coatings at $\omega = 50$ Hz and $A_0 = 248$ μm. Typical macroscopic coating using vibration-assisted convective deposition is shown in (a). The morphologies that result are submonolayer (b), monolayer (c), and multilayer depositions (d), shown as optical images partnered with analysis where blue particles are ordered, red particles have fewer than 6 nearest neighbors, and green particles have 6 nearest neighbors with asymmetric neighbor locations. SiO_2 microspheres are surrounded by and packed within polystyrene nanoparticles (e).

with water-substrate contact angle up to 80° including GaN, polyethylene terephthalate, and Fluorine-doped Tin Oxide (FTO) surfaces can be coated easily; traditionally, convective deposition is limited to highly wettable substrates. Although these effects are not quantified, they are readily apparent when using this technique in application.

Similar to traditional convective deposition, at the meso-scale, three surface morphologies are observed: submonolayer, monolayer, and multilayer depositions (Figs. 2(b)–2(d), respectively). Depending on experimental conditions, samples may be comprised of a single morphology or may exhibit all three deposited in a periodic manner in the direction of deposition. Locally, microspheres are in contact and the interstitial regions between particles are filled with nanoparticles. Experimental conditions are tuned such that microspheres and nanoparticle are codeposited; neither component will be deposited alone and void spaces have neither microspheres nor nanoparticles.[23,24]

Significant enhancements resulting from the addition of vibration are exhibited in the phase diagram (Fig. 3). Non-vibrated samples, exactly replicating traditional convective deposition, on the y-axis show that a single condition generates a monolayer. The addition of vibration yields two primary effects. First, for all A_0 sampled, the monolayer deposition speed is increased. It can be interpreted that the effective length, l, of the thin film is increased similar to that seen in laterally vibrated evaporating droplets of water, where the evaporation is enhanced near the contact line. Second, there is a wide monolayer deposition range of conditions. For $\omega = 1$ Hz, a small region spanning less than 10 μm/s results in monolayer coatings near 20 μm; at high amplitude, no long range monolayer deposition condition exists. At $\omega = 10$ Hz, results are similar to $\omega = 1$ Hz, but the range of monolayer deposition rates is roughly twice as large. For higher frequencies, the range of conditions resulting in monolayer depositions increases drastically and is no longer limited to small amplitude vibration. With $\omega = 20$ Hz and $\omega = 50$ Hz, increases/decreases to deposition speed by as much as ~50% do not necessarily transition deposition conditions beyond the monolayer regime, suggesting the mode of deposition has drastically changed.

Through dimensional analysis, one can consider the relative effects of inertia, surface tension, and viscosity. The Reynolds number, $Re = \rho u L/\mu$, relating inertial to viscous forces increases roughly 100-fold with vibration addition. However, it is still no more than $O(10^{-2})$ and thus is far below instability conditions for thin film flow. The capillary number, $Ca = \mu u/\gamma$, relating viscous to surface force also increases by roughly 100-fold; however, it also remains extremely small at $O(10^{-4})$. The Weber number, $We = \rho A_0 \omega^2 L^2/\gamma$, is $O(10^{-3})$ when based on the millimeter scale radius of curvature of the droplet between the blade and substrate. Although drop breakup is associated with We roughly O(1), this amount of inertia is sufficient to alter the shape of a droplet. Here, the suspension interface likely deforms due to lateral acceleration. This deformation would create pressure variations within the thin film that significantly alters the flow profile. Particles sliding over the substrate may sustain lubrication with respect to the substrate, increasing the time which they can assemble before being brought into contact with the substrate through capillary force.

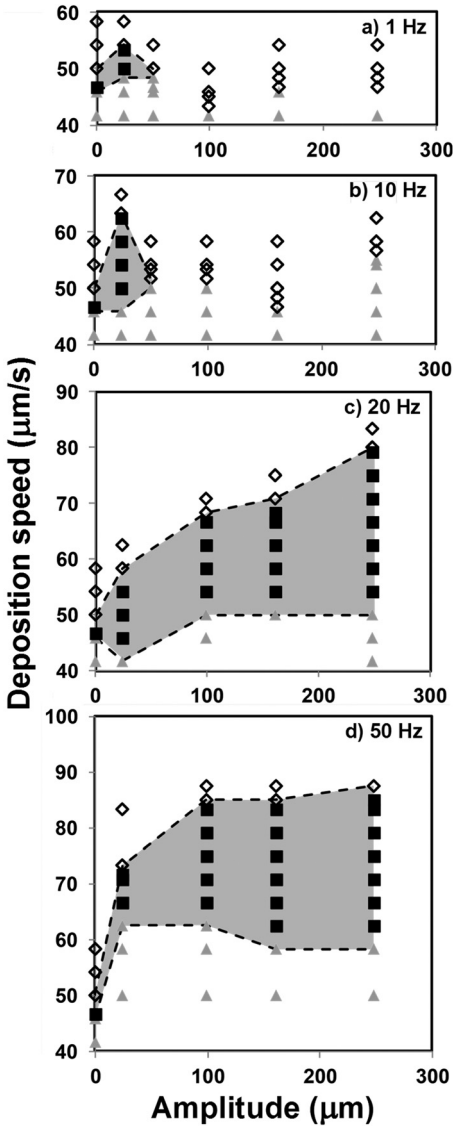

FIG. 3. Phase diagrams show the resulting morphology as a function of changing amplitude, A_0, and deposition speed for w = 1, 10, 20, and 50 Hz. Open diamonds represent submonolayer deposition, black squares are monolayer conditions, and grey triangles are multilayer depositions. The operating conditions for monolayer deposition are shaded in grey to guide the eye.

The two-dimensional packing density and local order in monolayer depositions are enhanced by vibration as well. Fig. 4 shows compiled microstructural analyses. There is small variation in sample quality within the monolayer regime. In all samples, this vibration-induced reduction of deposition speed sensitivity results in smaller error bars. Particles likely have more relative time within the thin film to assemble before capillary forces pin the particles to the substrate. Further investigation is necessary to determine the specific changes in self-assembly within the thin film.

We have demonstrated a significant enhancement to particle convective deposition that enhances surface density and local order of monolayers, increases viable deposition rate, and reduces the sensitivity of surface morphology to deposition speed without changing particle, solvent, or surface chemistry. No previous study has shown methodology to reduce the sensitivity of deposited morphologies to deposition speed. This relatively simple alteration to traditional

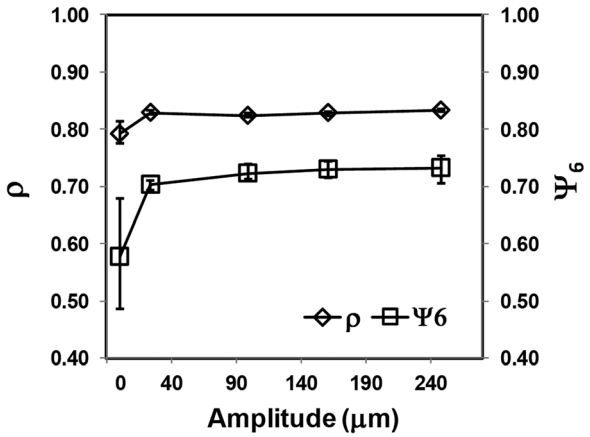

FIG. 4. Surface density, ρ, and local order parameter, Ψ_6, as a function of vibration amplitude for $w = 50$ Hz. Surface density and order increase as compared to traditional convective deposition, $A_0 = 0$, and smaller error bars indicate less variability between samples.

convective deposition may also be extended to dip coating and other systems where assembly occurs in flowing thin films.

This material is based upon the work supported by the National Science Foundation Scalable Nanomanufacturing Program under Grant No. 1120399. T.M. gratefully acknowledges support through the Royal Thai Scholarship Program.

[1]P. Kumnorkaew, Y. K. Ee, N. Tansu, and J. F. Gilchrist, Langmuir **24**, 12150 (2008).
[2]Y. K. Ee, R. A. Arif, N. Tansu, P. Kumnorkaew, and J. F. Gilchrist, Appl. Phys. Lett. **91**, 221107 (2007).
[3]Y. K. Ee, P. Kumnorkaew, R. A. Arif, H. Tong, H. Zhao, J. F. Gilchrist, and N. Tansu, IEEE J. Sel. Top. Quantum Electron. **15**, 1218 (2009).
[4]Y. K. Ee, P. Kumnorkaew, R. A. Arif, H. Tong, J. F. Gilchrist, and N. Tansu, Opt. Express **17**, 13747 (2009).
[5]X. H. Li, R. Song, Y. K. Ee, P. Kumnorkaew, J. F. Gilchrist, and N. Tansu, IEEE Photon. J. **3**, 489 (2011).
[6]X. H. Li, P. Zhu, G. Liu, J. Zhang, R. Song, Y. K. Ee, P. Kumnorkaew, J. F. Gilchrist, and N. Tansu, J. Disp. Technol. **9**, 324 (2013).
[7]A. L. Weldon, P. Kumnorkaew, B. Wang, X. Cheng, and J. F. Gilchrist, ACS Appl. Mater. Interfaces **4**, 4532 (2012).
[8]B. Wang, A. L. Weldon, P. Kumnorkaew, B. Xu, J. F. Gilchrist, and X. Cheng, Langmuir **27**, 11229 (2011).
[9]A. B. Pawar and I. Kretzschmar, Macromol. Rapid Commun. **31**, 150 (2010).
[10]R. D. Deegan, O. Bakajin, T. F. Dupont, G. Huber, S. R. Nagel, and T. A. Witten, Nature **389**(6653), 827 (1997).
[11]M. Yamaki, J. Higo, and K. Nagayama, Langmuir **11**, 2975 (1995).
[12]A. S. Dimitrov and K. Nagayama, Chem. Phys. Lett. **243**, 462 (1995).
[13]B. G. Prevo and O. D. Velev, Langmuir **20**, 2099 (2004).
[14]W. A. Gifford and L. E. Scriven, Chem. Eng. Sci. **26**, 287 (1971).
[15]D. Vella and L. Mahadevan, Am. J. Phys. **73**, 817 (2005).
[16]D. D. Brewer, J. Allen, M. R. Miller, J. M. de Santos, S. Kumar, D. J. Norris, M. Tsapatsis, and L. E. Scriven, Langmuir **24**(23), 13683 (2008).
[17]V. I. Baikov, A. T. Listrov, and Z. A. Shabunina, J. Eng. Phys. **43**, 1413 (1982).
[18]R. J. Bauer and C. H. von Kerczek, J. Appl. Mech. **58**, 278 (1991).
[19]S. J. Weistein, J. M. Baumlin, and J. Servant, AIChE J. **39**, 1113 (1993).
[20]O. V. Rudenko, A. I. Korobov, B. A. Korshak, P. V. Lebedev-Stepanov, S. P. Molchanov, and M. V. Alfimov, Nanotechnol. Russia **5**, 469 (2010).
[21]M. Alvarez, J. R. Friend, and L. Y. Yeo, Langmuir **24**, 10629 (2008).
[22]Q. H. Wei, D. M. Cupid, and X. L. Wu, Appl. Phys. Lett. **77**, 1641 (2000).
[23]P. Kumnorkaew and J. F. Gilchrist, Langmuir **25**, 6070 (2009).
[24]P. Kumnorkaew, A. L. Weldon, and J. F. Gilchrist, Langmuir **26**, 2401 (2010).